2021 18th Annual IEEE International Conference on Sensing, Communication, and Networking (SECON) | 978-1-6654-4108-7/21/$31.00 ©2021 IEEE | DOI: 10.1109/SECON52354.2021.9491583

Software-Defined Visible Light Networking for Bi-Directional Wireless Communication Across the Air-Water Interface

Kerem Enhos, Emrecan Demirors, Deniz Unal and Tommaso Melodia
Institute for the Wireless Internet of Things, Northeastern University, Boston, MA, U.S.A.

***Abstract*—Autonomous networks of sensors, unmanned aerial vehicles (UAVs) and unmanned underwater vehicles (UUVs) will play a vital role in scenarios/applications where a plethora of distributed assets across multiple domains – air and water - operate in unison to accomplish a common goal. However, establishing high data rate, robust, and bi-directional communication links across the air-water interface between aerial and underwater assets is still an open problem. In this article, we propose a communication system based on visible (blue) light that enables aerial and underwater assets to establish bi-directional links through the air-water interface without requiring any pre-existing communication infrastructure such as buoys acting as relay nodes. We first derive a mathematical model and accordingly build a simulator for the bi-directional air-water visible light communication (VLC) channel accounting for water surface distribution, optical parameters and path losses. Then, we design and prototype a software-defined visible light communication (VLC) modem. We present an extensive experimental evaluation conducted both in a test tank and in the ocean using the proposed VLC modem prototypes.**

***Index Terms*—Visible Light Communication, Inter-medium Communication, Air-Water Interface, Software-Defined Modem.**

I. Introduction

Networks of sensors, unmanned aerial vehicles (UAVs) and unmanned underwater vehicles (UUVs), composed of autonomous and wirelessly connected aerial and underwater devices, will play a key role in scenarios/applications where distributed assets in multiple domains – air and water - operate in unison to accomplish a common goal. Such networks of heterogeneous assets would enable numerous present and future military and civilian applications including but not limited to (i) offshore oil and gas exploration and infrastructure monitoring [1]; (ii) tactical surveillance [2], [3]; (iii) environmental monitoring (e.g., climate change, pollution tracking, marine life) [4], [5]. However, how to establish a high data rate, robust, bi-directional communication link between aerial and underwater assets, across the air-water interface is still uncharted territory.

While there have been multiple research efforts over the recent years to fulfill this need, as discussed in Section II, there are still a number of open questions. As of today, the only viable way to establish a communication link between aerial and underwater assets is to deploy floating devices that are capable of relaying data. As shown in Fig. 1 (a), floating buoys equipped with both acoustic and RF communication capabilities have been widely used as gateways between underwater and terrestrial networks [6], [7]. Nevertheless, such floating buoy systems are vulnerable to environmental effects such as ocean dynamics (e.g., drifts, currents or surface waves) and harsh weather conditions. Moreover, in military or other critical applications, they can be easily detected, tampered with, jammed, or deactivated. Buoys may also significantly limit the operational area of aerial and underwater assets that are relying on them, as it may be prohibitive to deploy them vastly in terms of time and cost over large ocean areas. While using autonomous surface vehicles (ASVs) as gateways nodes could alleviate some of the deployment challenges like ocean dynamics, it is still far from addressing all the aforementioned limitations. An alternative approach to establish communication links between underwater and terrestrial networks is operating UUVs to continuously resurface and act as relays or data mules. Similar to relying on floating devices, using UUVs in such mode would substantially limit operational capabilities and raise severe security issues.

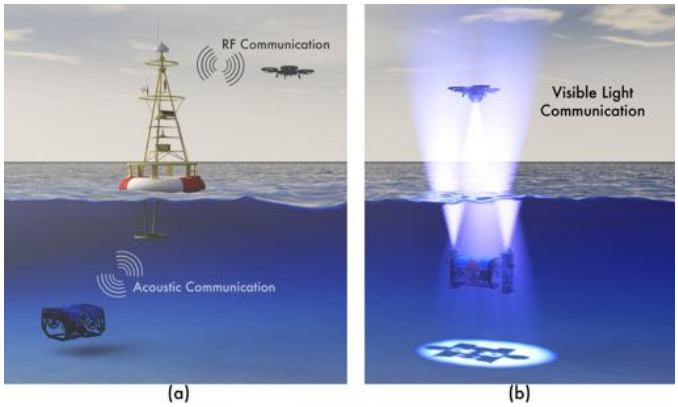

Fig. 1. *Communication Methods Across the Air-Water Interface:* (a) today, deploying a floating relay node (buoy system) is required. (b) the proposed visible light communication system that is establishing a bi-directional communication link between an UUV and an UAV through air-water interface without requiring any relay nodes.

To address these challenges, in this paper, as illustrated in Fig. 1 (b), we propose a communication system *enabling aerial and underwater assets to establish bi-directional links through the air-water interface, without requiring any relay nodes, using software-defined visible light networking*. The proposed communication system is based on a software-defined radio (SDR) paradigm to provide both aerial and underwater nodes with robust, secure, and self-optimizing communication functionalities for operating in temporally and spatially varying and potentially contested environments. In this paper, we make the following core contributions:

- **Modeling of Optical Propagation of the Air-Water Interface.** We derive a mathematical model of the visible light channel across the air-water interface to characterize the limitations imposed by the water surface distribution, optical properties and path loss. Specifically, we investigate the effects of distance, misalignment between transmitter and receiver, water surface waves, and water clarity. Accordingly, we build a simulator that can generate 3D channel models to evaluate

This work was supported by the National Science Foundation under Grant CNS-1763964 and Grant CNS-1726512.

these effects (Section III);

• **Visible Light Software Defined Modem.** We design and prototype a software-defined visible light communication (VLC) modem based on a reconfigurable System-on-Chip (SoC) architecture incorporating a field programmable gate array (FPGA) and a general purpose processing unit. Moreover, we design and prototype a visible light front-end including (i) a LED driver circuitry and $465\,\mathrm{nm}$ blue LEDs on the transmitter chain; (ii) a silicon avalanche photodetector with high responsivity at blue light band $(450-480\,\mathrm{nm})$ and a variable gain amplifier (VGA) on the receiver chain (Section IV);

• **Extensive Experimental Campaign.** We conduct an extensive experimental evaluation campaign in a test tank and in the ocean to evaluate the performance of the developed software-defined VLC modem. First, we test different modulation schemes and compare their performance under different noise conditions (Section V-A). Then, we test and observe the effects of distance, misalignment, water clarity, surface waves, and background noise to the performance of the proposed communication system (Section V-B). Furthermore, we cross-validate the experimental results with the simulation results obtained from the developed simulator (Section III). Finally, we conduct a set of experiments in the ocean to demonstrate that the proposed software defined VLC modem can communicate through the air-water interface bi-directionally "in-the-wild" (Section V-C).

II. Related Work

Multiple research efforts have been attempted to enable communications through the air-water interface in recent years. In this section, we review them under two main categories: optical communications and alternative approaches.

Optical Communications. Underwater optical communication has been a widely studied research area, primarily to offer a high data rate, short range alternative to underwater acoustic communications [8], [9]. Earlier works on underwater optical communications mainly leveraged lasers [10]. While laser-based solutions were proven to provide high data rate ($>1\,\mathrm{Mbits/s}$) over short distances ($<30\,\mathrm{m}$), their highly directional nature and requirement for high precision in pointing the beams were limiting their practical use. To overcome these constraints, more recently, the use of diffused light sources such as LEDs has been proposed [11], [12]. Thanks to the relatively low attenuation levels in the blue-green band ($(400-500\,\mathrm{nm})$ in the ocean/sea water [13], there has been a large body of work leveraging LED sources and receivers operating at these visible light frequencies [14]–[17], including commercial systems such as Sonardyne's BlueComm [18]. Readers are referred to the following surveys for a more detailed overview on underwater optical communications [10], [19], [20].

Despite the numerous works leveraging optical communications for the underwater environment, there have been only a few studies focusing on optical communications across the air-water interface. In [21], [22] Sun *et al.* attempted to establish unidirectional communication links across the air-water interface. Particularly, the paper focuses on demonstrating optical transmission from underwater to air by leveraging LEDs or diffused laser diodes. While the manuscript presents some promising results in terms of data rates (up to $850\,\mathrm{Mbit/s}$), they only consider unidirectional links, limited coverage areas (up to $0.1963\,\mathrm{m}^2$) and small, impractical wave heights (up to $1.5\,\mathrm{cm}$) during their studies. Moreover, the presented testbed heavily depends on bench-top components which is further limiting its practicality. On the other hand, Islam *et al.* [23] present a comprehensive study on using optical wireless communication to establish a unidirectional robust link between underwater receiver nodes and airborne transmitter devices. Although [23] provides an extensive analysis on the light intensity and validation results based on simulations and flat surface lab experiments, it does not focus on the wireless link performance or the bi-directional link across air-water interface.

Chen *et al.* [24] present a controlled testbed of $26\,\mathrm{m}$ air-water channel ($21\,\mathrm{m}$ water $5\,\mathrm{m}$ air) with $520\,\mathrm{nm}$ OFDM modulated laser diodes providing $5.5\,\mathrm{Gbps}$ with 2.47×10^{-3} bit-error-rate (BER) performance. However, because of the precise orientation requirements of a laser diode and a photodetector, the system would have limited practical use in the presence of high current and wavy water surface. By considering this limitation, Nabavi *et al.* [25] construct a channel model for the air-water interface communication including numerical analysis and simulations conducted for single photon avalanche diode (SPAD) receivers. Similarly, in [26], empirical validation of the air-water channel is done by using PIN photodiodes and white phosphorous LEDs under different turbulent water surface conditions and impulse response of the air-water channel is obtained. In addition, in [27], an air-water impulse response considering the effects different wind speeds and ocean currents is simulated.

Alternative Approaches. A few recent papers have focused on alternative approaches to communicate across the air-water interface. Tonolini *et al.* [28] propose a new communication technique called Translational Acoustic-RF Communication (TARF), which uses RF radars to detect physical displacements on the water surface created by acoustic waves using an acoustical waterborne transducer. While TARF stands out as a promising alternative technology, it can only support unidirectional communication (water to air) and operate in the presence of surface waves up to $16\,\mathrm{cm}$. Low data rate support ($400\,\mathrm{bps}$) and requirement for a precise alignment of the transmitter and receiver pairs are also some other limitations of the proposed technology. Another approach that is presented in the literature for communicating through the air-water interface is using magnetic induction (MI) [29], [30]. Even though a smooth transition across the interfaces can be maintained thanks to the similar magnetic permeability of air and water mediums, due to the conductance of salty water, high attenuation limits the communication range severely.

This work separates itself from prior work by enabling bi-directional visible light communication across the air-water interface by using a software-defined modem with a custom built VLC front end. The flexible nature of the software-defined architecture ensures successful communication in various environmental conditions such as high wave height, turbidity, background noise, among others. Vacuum sealed encapsulation enables the deployment of modems underwater, which is often overlooked in prior work.

III. Air-Water Visible Light Channel Model

Modeling of the air-water VLC channel is vital to characterize the system capabilities and define the limitations imposed by the water surface distribution, optical properties and path loss. After obtaining the necessary parameters that affect communication through the air-water interface channels, modeling can guide the design of communication systems and shed light on the performance to be expected.

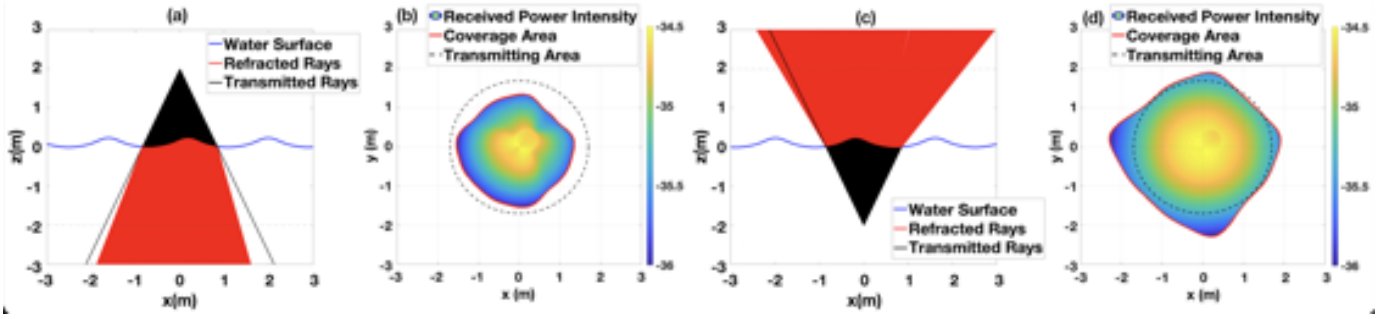

Fig. 2. Plots are generated with the simulation model and $t = 1.1$ sec, $d_{air} = d_{water} = 2$ m. Light path graphs ((a) and (c)) are shown for only $\varphi = 0°$ of the cylindrical coordinate system. Illumination area graphs ((b) and (d)) are shown for the depth at d_{water}. Parameters of the water surface function is $ka = 0.4$, $\lambda = 1.8$, and wave height, $H = 25$ cm.

A. Mathematical Modelling

We first derived a mathematical model for the water surface, which is the main factor affecting propagation in an air-water interface communication channel. We modelled the surface wave with a third-order Stokes' wave [31]. Through that model, we determined the water surface elevation for different horizontal coordinates at different times. Consequently, we geometrically calculated each ray of light's trajectory to determine the coverage area that can be illuminated by a VLC transmitter with a ray tracing approach. To perform accurate trajectory calculations, we account for the water surface model generated, the distances of transmitter and receiver above and below the water surface, d_{air} and d_{water} respectively and field of view of the transmitting source. We first derived the incident angle by calculating the angle between the transmitted ray and the orthogonal slope of the tangent of the water surface. Then by using the Snell's law, we calculated the refraction angle. Lastly, by calculating the slope of the refracted ray, we determined the horizontal coordinate of the incident ray at the depth of receiver. To extend the coverage area results into a 3D surface area, we repeated the trajectory calculations for each azimuth angle in a cylindrical coordinate system.

Finally, we calculated the light intensity (irradiance) inside the coverage area determined by accounting for the path loss imposed by the air-water interface. We first calculated the irradiance at the water surface through the inverse square law. Then, at the water surface, we used the Fresnel equations to calculate the amount light penetrating into the water medium. Inside the water medium, two components of path loss are effective. The first is the beam attenuation caused by the absorption and scattering of water while the second is the geometric loss, caused by the spreading of the beam over the traveling distance of light [32]. Considering all path loss components, we obtained the received light intensity, at a specific point in the cylindrical coordinate system. The detailed equations for the mathematical modelling can be found in the Appendix.

B. Channel Simulator

Leveraging the channel model developed, we implement a VLC channel simulator for the air-water interface. Specifically, the simulator is realized through MATLAB and is capable of simulating 3D air-water VLC channels. As an example, as presented in Fig. 2 (a) and (c), a VLC channel for a water surface with $25\,\mathrm{cm}$ waves present, is simulated through the simulator developed. Coverage area and irradiance calculations for each cases of air-to-water (A2W) and water-to-air (W2A) channels are simulated for each azimuth angle as shown in Fig. 2 (b) and (d). The coverage areas that would occur if there were no air-water medium transitions in the channel are shown with black dashed lines (labelled as transmitting area). Because of the refractive index difference between two mediums, for the A2W case the coverage area is smaller than the transmitting area while for the W2A case the coverage is larger than the transmitting area. As it can be observed from this toy example, the simulator developed is capable of providing irregularity of the coverage area boundaries, light intensity distribution at varying temporal and spatial settings. Since calculation of incident illumination intensity at specific distance can be achieved with this simulator, with known transmitted electrical power of the light source and the noise level of the receiver, signal-to-noise ratio (SNR) can be obtained for the desired channel setting. Thus, for different environmental conditions, channel configurations, and position of aerial or underwater assets, the simulator enables preforming link and network level evaluations. Furthermore, the simulator can guide and feed vital insights to the network operators or automatic control algorithms for deploying the multi-domain assets efficiently to achieve the best operational results.

IV. Software-Defined VLC Modem

In this section, we introduce the software-defined VLC modem that is designed and built based on the software-defined radio (SDR) paradigm for providing robust, secure, and self-optimizing communication functionalities in temporally and spatially varying and potentially contested environments. The designed modem incorporates three main modules: main module, power and switch module, and VLC front-end, as shown in Fig. 3.

Main Module. The main module incorporates a MicroZed Xilinx Zynq-7000 programmable system-on-chip (SoC) integrating FPGA and ARM processor on a single substrate. Through the combination of ARM processor and FPGA, the modem's main module can provide hardware and software reprogrammability with compact packaging and low energy consumption. The main module also houses analog-to-digital and digital-to-analog converters for transmitting and receiving signals from the VLC front-end. Specifically, a LTC1740CG ADC with $14-$bit parallel outputs supporting $6\,\mathrm{Msample/s}$ and a LTC1668 DAC operating on $16-$bit parallel inputs with $50\,\mathrm{Msample/s}$ are used in the main module.

Power and Switch Module. The power and switch module has two main functionalities in the modem design. First, it interfaces the modem to a battery unit through PCI-Express connectors. It also integrates a surge suppression circuitry for avoiding any surges. Power is supplied through a Lithium-ion battery, which is capable of supplying $14.8\,\mathrm{V}$, $18\,\mathrm{Ah}$. The module incorporates multiple voltage regulators to provide each individual module with different voltages (e.g.,$\pm 5\,\mathrm{V}$ and

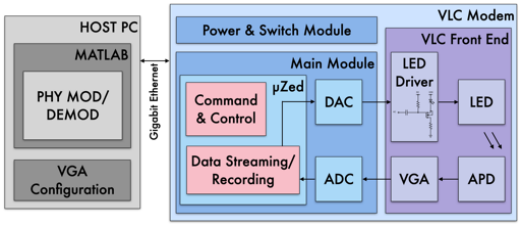

Fig. 3. Block diagram of software defined VLC modem.

± 15 V). Second, the module incorporates a set of connectors for carrying analog and digital signals between different modules. Particularly, it interfaces main module to the VLC front-end to facilitate visible light communications.

VLC Front-End. The VLC front-end includes a LED driver on the transmitter side. The driver is composed of a single n-channel MOSFET (TI CSD18535KTT) with common source topology with source degeneration. The AC input signal is biased with an appropriate DC level to turn on the transistor. This DC bias is supplied to the LED driver by the switch module, which supplies 3.3 V TTL level DC bias when the transmission command is generated through the main module. In this way, LED can be turned off when a VLC transmission is not occurring. Instead of amplifying the current outputted from the DAC, due to the limited output current, a voltage controlled current source is implemented by using MOSFET. Thus, the current on the load on the drain pin of the MOSFET, which is LED in this case, is controlled by the voltage at the gate of the MOSFET. The maximum current drain is also limited with the resistor on the source pin of the MOSFET. Finally, this voltage controlled current source is driving four series connected LEDs (OSRAM OSLON SLL 80 GBCS8PM $465\,\mathrm{nm}$ blue LED) that are connected in series on drain of the MOSFET. Each LED is driven with current of 1 A peak-to-peak. Thus, each LED outputs average power of 1.5 W, with typical radiant flux of $727\,\mathrm{mW}$.

On the receiver side, the VLC front-end uses a silicon avalanche photodetector (Thorlabs APD430A2) for receiving light signals. The specific photodetector is chosen because of its high responsivity at blue light band $(450 - 480\,\mathrm{nm})$ and high transimpedance bandwidth $(400\mathrm{MHz})$. The photodetector has built-in transimpedance amplifier, whose gain can be controlled with a knob. Although the amplification factor is not defined in its datasheet, for all the experiments in this work, transimpedance gain is kept at the maximum setting possible. After I-V conversion inside the photodetector, signal is amplified by an AD8330 variable gain amplifier (VGA). Gain of this preamplifier can be controlled digitally by the main module varying gain values between $0 - 50$ dB. VLC front-end is operated through a custom built PCB, which incorporates LEDs, LED driver, and photodetector. VGA circuit is built on a separate PCB which is connected as a bridge between the power and switch module by using PCI Express connectors. Connection between the VLC front end and other modules are supplied through micro-coaxial cables.

The software-defined VLC modem is designed to be operated in two modes. In the first mode, it can operate as a full-blown VLC modem executing software-defined communication protocol stack on the Zynq SoC. In the second mode, it can operate similar to a COTS software-defined radio platform where the protocol stack is implemented on a Host PC connected to the VLC modem via an Ethernet connection. Specifically, in this mode, the VLC modem allows host computer to control, stream and record data through VLC front-end. For rapid prototyping and testing purposes, in the experimental evaluation of this paper, the VLC modem will be operated as an SDR platform where it will be commanded via a secure shell protocol over Ethernet as shown in Fig. 3. For the experiments, the software-defined VLC modem's hardware is encapsulated by using 4" cylindrical acrylic pressured enclosure, as shown in Fig. 4. Tubes are vacuumed in order to increase the outside pressure of the tube to intensify the compression of the encapsulation. Ethernet and power are supplied through custom $10\,\mathrm{m}$ length waterproof cables.

V. Experimental Results

In this section, we present the results on the different sets of experiments conducted both in a water test tank (with dimensions of $3\mathrm{m} \times 1.5\mathrm{m} \times 1\mathrm{m}$) and in the ocean leveraging the developed software-defined VLC modems. First, we test different modulation schemes and compare their performance under different channel conditions across the air-water interface in Section V-A. Then, we test and report on the effects of distance, misalignment, water clarity, surface waves and background noise to the performance of the VLC modems communication across the air-water interface in Section V-B. Moreover, we cross-validate the experimental results with the simulation results obtained from the simulator developed in Section III. Finally, we conduct a set of experiments in the ocean to showcase that the proposed system can operate "in-the-wild" in Section V-C.

A. Modulation Scheme Analysis

In this section, we compare different modulation schemes implemented on the software-defined VLC modem over a bi-directional air-water channel in terms of the BER performance. Unlike RF or acoustic communication systems where modulation schemes can leverage amplitude, frequency, and phase, in VLC systems, the intensity of the light is modulated. Such modulation schemes are referred as intensity modulation and direct detection (IM/DD) schemes. In this work, we implement and compare both single carrier modulation schemes (i.e., On-Off keying (OOK)) and multi carrier modulation schemes (i.e., Carrierless Amplitude and Phase Modulation (CAP) and

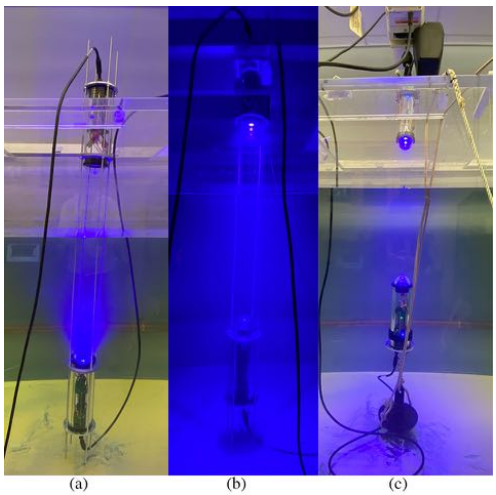

Fig. 4. Testbed configurations for different analysis. In (a) and (b) VLC modems are prealigned and both W2A and A2W transmission is shown respectively. In (c) one VLC modem is hanged on a crane that can move in horizontal and vertical directions and the other modem is fastened with a small mushroom anchor underwater.

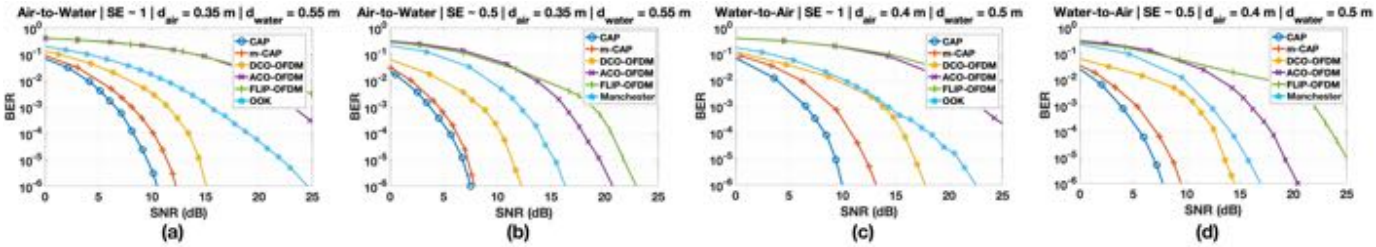

Fig. 5. BER analysis for both air-to-water and water-to-air configurations with spectral efficiencies of 1 and 0.5 bit/s/Hz. Five sub-bands are used for m-CAP scheme. Utilized bandwidth is equal for each experiment.

Orthogonal Frequency Division Multiplexing (OFDM)) which are commonly used in underwater VLC systems [20].

Single Carrier Modulation Schemes. OOK is the simplest and most intuitive solution for IM/DD in VLC, as high or low light intensity represents the incoming binary data bits. A simple modification applied to OOK is called Manchester Encoding (ME). Although this encoding requires twice the bandwidth, it is less susceptible to noise compared to OOK. Hence, spectral efficiencies of OOK and ME schemes are inherently 1 and $0.5\,\mathrm{bit/s/Hz}$ respectively.

Multi Carrier Modulation Schemes (MCM). CAP stands out as a spectrally efficient multi carrier modulation scheme widely used in VLC. CAP scheme enables the trade-off between spectral efficiency and BER performance through adjusting its parameters (e.g., span, samples-per-symbol (SPS), roll-off factor, etc.) and can provide better peak to average power ratio (PAPR) and BER performance compared to other multi carrier schemes [33]. Multi-band CAP (m-CAP) scheme can be established by summing up multiple CAP scheme waveforms applied with different center frequencies of pulse-shaping filters. Optical OFDM is also a widely adopted scheme in VLC, thanks to its robustness against inter-symbol interference (ISI) and multipath fading. Unlike its RF-based counterparts, Optical OFDM schemes cannot use complex-valued bipolar signals. To address that, two major variants of OFDM schemes are widely adopted [34]. First is called DC-biased Optical OFDM (DCO-OFDM), which converts bipolar signals to usable unipolar signals by adding DC offset. The latter is called Asymmetrically Clipped Optical OFDM (ACO-OFDM) which adopts a computational technique that uses only odd subcarriers. Similar variation to ACO-OFDM is called FLIP-OFDM. Although it depends on transmission of positive and negative components in two consecutive symbols, FLIP-OFDM offers the same spectral efficiency as ACO-OFDM.

For a fair comparison between single and multi carrier modulation schemes, OOK and ME are compared separately with MCM. Spectral efficiencies of MCM schemes are configured to be comparable with the stated single carrier modulation schemes.

Experimental Results. In this set of experiments, OOK, CAP, m-CAP ($m = 5$), DCO-OFDM, ACO-OFDM, and FLIP-OFDM are implemented and tested. For rapid prototyping and testing purposes, each modulation scheme is implemented as MATLAB scripts and generated waveforms are fed into VLC modems' FPGA via a secure shell protocol over Ethernet as described in Section IV. In this set of experiments, 1 MHz of bandwidth is utilized. To obtain a fair BER comparison between different modulation schemes, the parameters of all multi carrier schemes (i.e., CAP and OFDM) are adjusted to the minimum possible modulation order. In all OFDM schemes, FFT size is selected to be 64 and channel equalization is done by using $N_S/4$ number of pilots, where N_S is the number of total subcarriers. For achieving packet detection and synchronization, each data packet is preceded by a $511-$length pseudo-noise (PN) sequence preamble. During the experiments, two VLC modems are pre-aligned with a 6 ft aluminum rod in a water test tank, as it can be seen from Fig. 4 (a), thus minimizing and fixing the pointing loss. It is important to note that all experiments are conducted for both air-to-water (A2W) and water-to-air (W2A) channels in a dark room and with flat water surface in order to eliminate other factors that can affect communication.

First, from Fig. 5, it can be observed that CAP and m-CAP outperforms all other modulation scheme in all communication directions (A2W or W2A) and spectral efficiencies. For ACO- and Flip-OFDM schemes, due to their low bandwidth efficiency, modulation order was set to $16-$QAM and $4-$QAM for spectral efficiencies of 1 and $0.5\,\mathrm{bit/s/Hz}$ respectively, which results in relatively worse performance. Thus, DCO-OFDM is the best performing OFDM-based scheme. Even though DCO-OFDM needs higher SNR at same BER compared to CAP modulation, it still outperforms OOK in every configuration.

It is also observed that communication direction (A2W or W2A) has no substantial effect on the BER performance of different modulation schemes. More specifically, for each modulation scheme, at same BER, required SNR level increases approximately 1 dB, if configuration is W2A instead of A2W. This is mainly due to the reflection and scattering underwater. Thus, due to total internal reflection, portion of light rays that can penetrate to air medium decreases. However, for A2W case, all the light rays with irradiance angle less than $90°$, can penetrate to water medium, where the intensity of light increases by means of reflections inside the water medium.

After comparing all the modulation schemes for VLC across the water surface, it is shown in Fig. 5 that CAP and DCO-OFDM outperforms others in both configurations and different spectral efficiencies. For DCO-OFDM, PAPR is measured to be 11.25 dB and 12.56 dB for spectral efficiencies of 1 and $0.5\,\mathrm{bit/s/Hz}$ respectively. While for CAP, these values decrease to 4.41 dB and 6.75 dB. However, for 5-CAP, PAPR values measured to be the highest among these schemes as 12.55 dB and 14.33 dB. Moreover, in Fig. 6, CAP, 5-CAP and DCO-OFDM are compared in terms of their maximum feasible data rate (BER vs Spectral Efficiency) for both A2W and W2A configurations. Although both configurations resulted in very similar outcomes, it is observed that DCO-OFDM can support higher data rates with better BER performance in the same given bandwidth.

B. Channel Analysis

In this set of experiment, a slightly different setup is used as shown in Fig. 4 (c). To observe the impact of distance and misalignment between VLC modems, horizontal (x-axis) and vertical (z-axis) distances are differentiated. Thus, one of

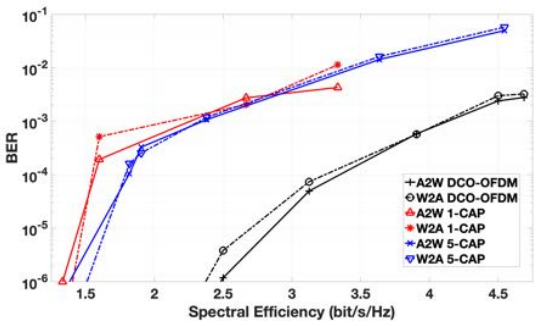

Fig. 6. Maximum feasible data rates for CAP, 5-CAP and DCO-OFDM schemes. Dashed lines are BER values for water-to-air VLC link and solid lines are for the air-to-water link.

the modems is attached to a crane that can move in these directions and the submerged modem is fastened to a small mushroom anchor keeping the modem at a fixed location. Length of the rope between the mushroom and modem can also be adjusted to vary d_{water}. In Section V-B1, d_{air} is increased with $0.05\,\mathrm{m}$ intervals by moving the crane vertically. These measurements are done iteratively for different distances between photodetector and water surface, d_{water} with $0.1\ \mathrm{m}$ intervals.

Similarly for a specific d_{air}, impact of misalignment between two modems can also be observed as in Section V-B2. The only difference is that the crane is moved horizontally. After aligning the transmitter and receiver modems in y-axis, crane moved in x-axis with $0.1\ \mathrm{m}$ steps while the submerged modem remained at the same point. In both A2W and W2A configurations modems are located with a distance of $0.42\mathrm{m}$ to the water surface unless otherwise stated. For Sections V-B3, V-B4, and V-B5, same pre-aligned setup that is used in Section V-A is used, as shown in Fig. 4 (a).

During this set of experiments, transmission power is kept at maximum and gain of the VGA on the receiver side is fixed. Hence, electrical noise level of the receiver is assumed to be equal for each configuration. In this way, despite of huge differentiation between the signal amplitude, contribution of the AWGN on the RMS value of the received signal remains the same. Incident optical power can be described as $P_{opt} = \frac{V_{out}}{\Re(\lambda)\times G}$, where V_{out} is the output voltage of the photodetector, $\Re(\lambda)$ is the detector's responsivity at a given wavelength, and G is the transimpedance gain. In Fig. 7-8, intensity is given in dB scale of W/m^2 units, which is also obtained from the irradiance calculations given in the Appendix.

1) Distance: Fig. 7 presents the experimental and theoretical results of the impact of distance on the irradiance (light intensity). Although experimental values are consistent with the theoretical values, some deviation is observed for the cases where the modem is placed within a distance to water surface less than $0.17\ \mathrm{m}$ for both A2W and W2A configurations. Also, it is observed that the light intensity is decreased by approximately $3\ \mathrm{dB}$ for W2A configuration, mainly due the total internal reflection.

As the developed simulation model is cross-validated through the experimental results, it is used for further estimating the maximum separation distance between the VLC modems based on SNR values. For the desired BER level, corresponding required light intensity, which can also be converted to a specific SNR value with the assumption of a constant AWGN, is known from Section V-A. Therefore, the required light intensity, which is obtained and validated through DCO-OFDM BER analysis under different noise

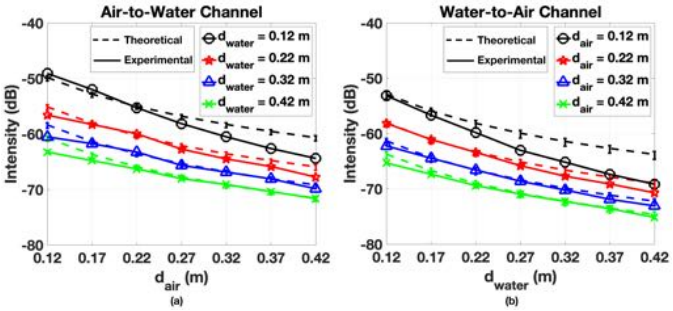

Fig. 7. Experimental results of the impact of distance variation on light intensity for air-to-water (a) and water-to-air (b) configuration is shown in solid lines. Theoretical values are also included in dashed lines for the purpose of validation of the implemented model.

conditions, for maintaining the maximum communication distance can be calculated by simulating the channel model. Considering that, the maximum separation distance for VLC modems to successful communicate with a BER less than 10^{-6} is calculated for each channel with our proposed system's power specifications. If the modem in air medium is placed at $d_{air} = 0.1\ \mathrm{m}$, maximum depth that the modem underwater can be placed is $d_{water} = 2.351\ \mathrm{m}$. Contrarily, if the modem underwater is placed at $d_{water} = 0.1\ \mathrm{m}$, maximum height that the modem in air can be located is $d_{air} = 2.403\ \mathrm{m}$. If the separation between the modems and water surface is equal, maximum communication distance is calculated as $d_{air} = d_{water} = 1.239\ \mathrm{m}$, which results in total of $2.478\ \mathrm{m}$.

2) Misalignment: In Fig. 8 (a), the impact of misalignment on the light intensity is shown for A2W communication link. It is observed that theoretical model is consistent with the experimental results for the misalignment values less than $0.2\ \mathrm{m}$. Since non-line-of-sight (NLOS) propagation is not included in the theoretical model, it is assumed that for regions larger than radius of $0.2\,\mathrm{m}$ is not illuminated. Since the water tank is small enough, considerable intensity of reflections can be gathered. Thus, in practice NLOS propagation contributes to received light intensity for coverage radius larger than $0.2\ \mathrm{m}$. Similar effect of NLOS propagation is observed for W2A communication link for misalignment distance larger than $0.28\ \mathrm{m}$. Due to refraction index difference, light propagating through underwater to air medium reflects with a higher irradiance angle compared to the transmission. Thus, the coverage area for W2A VLC links is higher compared to A2W communication.

Another observation is that even with the NLOS propa-

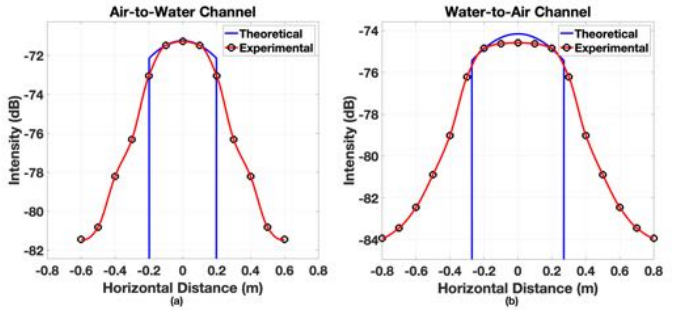

Fig. 8. Experimental results of the impact of misalignment on light intensity for air-to-water (a) and water-to-air (b) configuration is shown in black circle marker. In order to have a clearer visualization, data points are interpolated, as shown in red solid line. Theoretical values are also included in blue solid line for the purpose of validation of the implemented model.

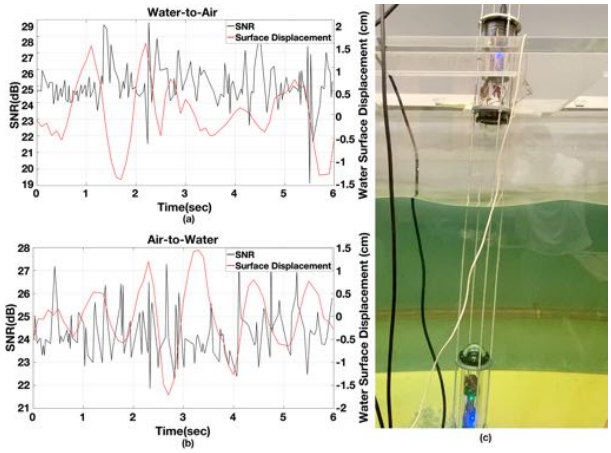

Fig. 9. Impact of water surface waves on water-to-air (a) and air-to-water (b) channels' signal to noise ratio. Instance of water surface wave in the experiment tank is also presented in (c).

gation, successful communication links can be maintained. For A2W configuration, BER remains less than 10^{-6} for a misalignment distance less than 0.4 m. However, for 0.5 m, BER drastically increases to 0.018. Similarly, for W2A configuration, this misalignment limitation for a communication link with less than 10^{-6} BER is increased to 0.7m. Again for 0.8m of misalignment, rapid increase of BER to 0.027 is observed. Thus, in practice, by taking into account NLOS propagation, misalignment limitation can be increased compared to the theoretical LOS links. Hence, the coverage areas for A2W and W2A links with given distance of 0.84 m between each modem (equally separated from water surface) are measured to be $0.5\,\mathrm{m}^2$ and $1.54\,\mathrm{m}^2$ respectively, while maintaining less than 10^{-6} BER.

3) Water Surface Waves: Another important factor impacting the VLC channel is the presence of surface waves. Until now all the measurements are conducted within a water tank with a flat water surface. However, in real ocean environment absolute flat water surface is unattainable. Thus, to examine the impact of water surface displacement on the received SNR, water surface inside the tank is disturbed to obtain waves.

Specifically, to obtain planar waves inside the tank, $60 \times 60\,\mathrm{cm}$ flat plastic object is used for thrusting the water. While establishing VLC link and generating waves, an Arduino module equipped with a acoustic distance sensor is used to record the water displacement. With this setup, maximum of 3 cm peak-to-peak water surface waves could be generated. While SNR differentiation of approximately 0.5 dB is observed for VLC with flat water surface, with the presence of waves, SNR is fluctuated for approximately ± 3.5 dB. Despite this huge fluctuation, VLC link is not obstructed and communication with less than 10^{-6} BER is maintained for both A2W and W2A configurations.

Although the generated waves are limited to $3\,\mathrm{cm}$, by using the simulation model (Section III), communication with different wave heights are simulated. In Fig. 2 (a) and (c), A2W and W2A channels with water surface height of 25 cm are simulated. It is shown that according to the received light intensity calculations, communication with less than 10^{-6} BER can be obtained, by comparing them to the experimentally received light intensity measurements.

4) Water Clarity: For all the other experiments, it is assumed that the water in the tank is clear, which is also proved with turbidity measurements ($0.09\,\mathrm{NTU}$). For reference, while drinking water standard is less than 1 NTU, ocean turbidity should not exceed 50 NTU according to the most of the state regulations in United States [35].

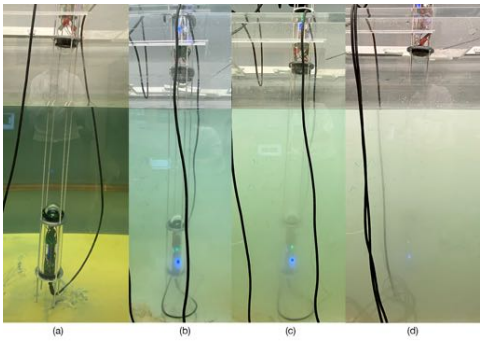

Fig. 10. Experiment tank with different concentrations of zinc oxide. For (a), zinc oxide is not present inside the tank where the turbidity is measured as 0.09 NTU. After adding zinc oxide to the water tank gradually, turbidity is measured as 1.71, 25.42, and 70 NTU for (b), (c), and (d) respectively.

In order to obtain water turbidity, zinc oxide is used. Zinc oxide is widely used for UV protection due to its obstructing effect on UV wavelength, while spectral transmission ratio for visible wavelength is higher than 90%. Thus, by using this material, turbidity of water is increased by generating suspending particles inside the tank, which creates particle scattering for the light rays traveling underwater without creating a spectral absorbance.

Concentration of zinc oxide is gradually increased with 25 gram steps and at every step received RMS values are recorded. Spectrophotometer is used to measure transmittance percentage and absorbance value that is used as the decadic attenuation coefficient for Beer-Lambert Law. While turbidity is measured in nephelometric turbidity unit (NTU), which cannot be converted into attenuation coefficient directly, this unit is used as a point of reference for quality of water. In Fig. 10, water tank with different turbidity levels are shown. As the concentration of ZnO increases, turbidity also increases and subsequently the submerged modem is not clearly visible after some point. Even though the turbidity level of 70NTU (Fig. 10 (d)) is much higher than the average allowed turbidity level in coastal waters, successful VLC link can still be established with the proposed VLC modem as presented in Table I.

It is observed that for A2W VLC link, experimental results validate the theoretical model (Fig. 11). However, as the attenuation coefficient or turbidity increases, experimental irradiance value starts to decrease slower than the theoretical values. This is caused by the assumption of Beer-Lambert Law. Beer-

TABLE I
BER AND WATER OPTICAL PROPERTIES (ABSORBANCE (A), TRANSMITTANCE (T), TURBIDITY (TU)) FOR DIFFERENT VALUES OF ZNO CONCENTRATION (C) ARE SHOWN.

C ($\mathrm{g/m^3}$)	A ($\mathrm{m^{-1}}$)	T (%)	TU (NTU)	BER A2W	BER W2A
0	5.00	89.1	0.09	$< 10^{-6}$	$< 10^{-6}$
16.78	5.41	88.4	0.36	$< 10^{-6}$	$< 10^{-6}$
33.57	6.01	87.0	1.71	$< 10^{-6}$	$< 10^{-6}$
67.14	7.00	85.3	25.42	$< 10^{-6}$	2.35×10^{-3}
117.49	9.01	81.0	64	6.2×10^{-5}	9.63×10^{-3}
142.67	9.61	80.3	70	2.11×10^{-3}	1.88×10^{-2}

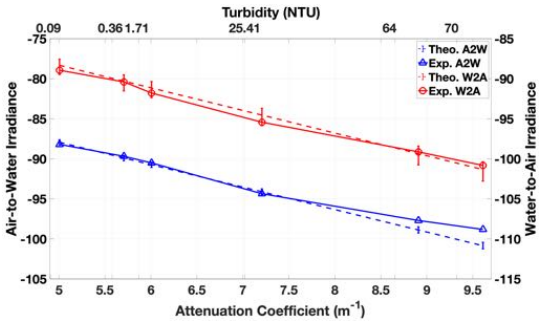

Fig. 11. Experimental results of the impact of water clarity on light intensity for air-to-water (a) and water-to-air (b) configuration is shown. Turbidity values corresponding to each attenuation coefficient is also given in NTU.

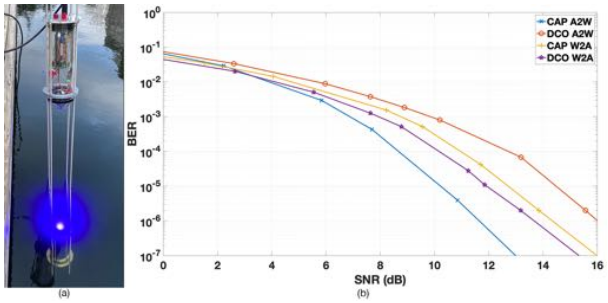

Fig. 12. (a) Experimental setup and water-to-air communication for ocean experiments. (b) BER analysis are conducted in coastal ocean water for both air-to-water and water-to-air configuration at ~ 1 Mbps for CAP and DCO-OFDM modulation schemes.

Lambert Law disregards the scattered photons that are collected by the photodetector. Thus, it is assumed that scattered photons are disappearing in the theoretical model, which is not the case in practice. Since, increase in ZnO concentration also increases scattering of the photons underwater, light rays that penetrates into water medium scatters. Scattered photons are also collected with the photodetector, which results in higher irradiance than the calculated values. For W2A configuration, experimental results hold with the theoretical model more accurately. Detection of scattered photons is not dominant as A2W configuration since the detector is in air medium, where scattered photons mostly remain underwater, unable to penetrate to air medium due to total internal reflection.

5) Background Noise: Until now, all the measurements were conducted in a dark room for eliminating the background noise factor (as shown in Fig. 4 (b). To quantify the effect of background noise, measurements obtained using fluorescent bulbs as the noise source. It is observed that indoor lighting (Fig. 4 (a) and (c)) decreases the SNR levels depending on the distance between transmitter and receiver modems for every modulation scheme. As the modems are separated by 0.82 m (equal distance to water surface), SNR level decreases by 2 dB. However, if the modems are as close as 0.24 m, SNR decrease is negligible. This is mainly due to the dominant transmitted optical power. If the modems are close to each other, received optical power intensity is dominated by the transmitted blue light. Contrarily, if the modems are separated from each other and background noise's irradiance becomes comparable to the transmitted optical signal, and accordingly received SNR decreases.

C. Ocean Experiments

In this set of experiments, two software-defined VLC modems used for conducting experiments in coastal ocean water. The goal of this experiments is to demonstrate that the proposed software defined VLC modem can establish bi-directional links through the air-water interface "in-the-wild". Particularly, in this set of experiments, both A2W and W2A channel configurations are tested with CAP and DCO-OFDM modulation schemes providing a 1 Mbit/s of data rate using a 1 MHz bandwidth.

As shown in Fig. 12 (a), in the ocean experiments, pre-aligned threaded aluminum rods are used for eliminating any misalignment loss and ease of control over the depth of the modem that is located underwater. Hence, distance between two VLC modems kept fixed 1 m during the experiments. The water clarity of the ocean water is investigated with spectrophotometer and absorbance and transmittance is measured to be 4.90 and 89.4% respectively. Fig. 12 (b) shows the obtained BER-vs-SNR performance results. It can be observed that the results are similar to the water tank experiments. For A2W configuration, CAP scheme outperforms DCO-OFDM at lower SNR values by maintaining lower BER, which is also seen in the tank experiments. Though, for W2A configuration, it is observed that DCO-OFDM performs slightly better than CAP. However, both modulation schemes can maintain communication at SNR values between $7 - 10$ dB for both communication links.

VI. Conclusions

We presented a communication system enabling aerial and underwater assets to establish bi-directional links through the air-water interface, without requiring any relay nodes, using software-defined visible light networking. We built a simulator generating 3D channel models for evaluating air-water interface. We also discussed a prototype of a software-defined visible light communication modem. We presented a detailed experimental evaluation both conducted in a test tank and at the ocean with the software-defined VLC modem prototypes. Particularly, we demonstrated the operational capabilities of the proposed system under different channel conditions.

Future research directions will include enhancing the prototypes in terms of bandwidth and gain capabilities and extending the prototypes to include FPGA implementations of different communication schemes as well as interfacing them with unmanned underwater and aerial vehicles.

Appendix

Notations in the expressions should be referred to Fig. 13. Surface water waves are composed of cnoidal waves, where third order Stokes' wave is suitable for such representation and defined as

$$\eta(x,t) = \alpha \left[\left(1 - \frac{1}{16}(k\alpha)^2 \right) \cos\theta + \frac{1}{2}(k\alpha)^2 \cos 3\theta \right], \quad (1)$$

where η is the free surface elevation as a function of the horizontal coordinate, x, and time, t. Also, $k\alpha$ is the wave steepness, α is the first order wave amplitude, and θ is defined as the wave phase, which is expressed as $\theta(x,t) = kx - wt$, where k is the wavenumber and w is the angular frequency.

In order to find the incident angle, θ_i, first orthogonal slope of the tangent of the water surface, m_{AB}, can be found by using the first derivative of $\eta(x,t)$. Then the slope of the incoming ray onto the water surface, m_{TW}, can be obtained by using the transmitter's position and the incident point of transmitted ray on the water surface. By using m_{TW} and m_{AB}, the incident angle can be calculated as

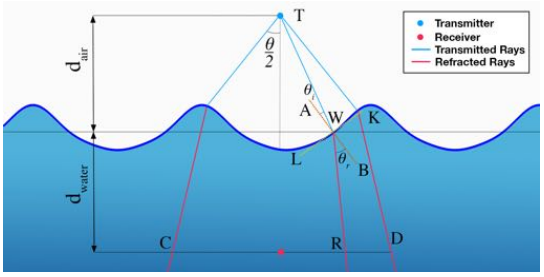

Fig. 13. Cnoidal shaped wave and demonstration of refraction of light rays.

$$\theta_i = \tan^{-1}\left|\frac{m_{TW} - m_{AB}}{1 + m_{TW} m_{AB}}\right|. \tag{2}$$

After obtaining the refraction angle, θ_r, by using Snell's law, the horizontal coordinate of the incident ray at the depth of the receiver, m_{WR}, can be calculated by quadratic expression (4), which is derived from (3) as

$$\tan\theta_r = \left|\frac{m_{AB} - m_{WR}}{1 + m_{AB} m_{WR}}\right|, \tag{3}$$

$$\begin{aligned}\left(m_{AB}^2 \cdot \tan\theta_r^2 - 1\right) \cdot m_{WR}^2 + 2 \cdot m_{AB}\left(1 + \tan\theta_r^2\right) \\ \cdot m_{WR} + \tan\theta_r^2 - m_{AB}^2 = 0.\end{aligned} \tag{4}$$

Considering all the path loss components, overall expression for the intensity of light for each incident ray at specific depth, where receiver is located can be calculated as

$$I = \frac{2\pi}{\theta}\frac{P}{4\pi \cdot d_{TW}^2} \cdot \tau \cdot e^{-c \cdot d_{WR}} \cdot \frac{(m+1)}{2\pi}\frac{A_R}{d_{WR}}\cos^m\phi, \tag{5}$$

where d_{WR} is the distance between the points of incidence on the water surface and at the depth of the receiver, and c (m^{-1}) is the beam attenuation coefficient, which is defined as the sum of absorption, a (m^{-1}), and scattering, b (m^{-1}), coefficients. Also, A_R is the photodetector area, ϕ is the angle of irradiance, which is equal to θ_r and m is defined as: $m = -1/\log_2(\cos\Phi_{1/2})$ where $\Phi_{1/2}$ denotes the angle at which the power falls to half.

REFERENCES

[1] Forbes, "Drones begin to deliver on their potential for the oil and gas sector," 2018, https://tinyurl.com/s8yo6ka9.

[2] ITNews, "Swarms of tiny robots could help defence clear underwater mines," 2020, https://tinyurl.com/39hvshzl.

[3] Forbes, "Robot motherships to launch drone swarms from sea, underwater, air and near-space," 2021, https://tinyurl.com/vsnynu4u.

[4] R. A. Armstrong, H. Singh, J. Torres, R. S. Nemeth, A. Can, C. Roman, R. Eustice, L. Riggs, and G. Garcia-Moliner, "Characterizing the deep insular shelf coral reef habitat of the hind bank marine conservation district (us virgin islands) using the seabed autonomous underwater vehicle," *Continental Shelf Research*, vol. 26, no. 2, pp. 194–205, 2006.

[5] J.-I. Watanabe, Y. Shao, and N. Miura, "Underwater and airborne monitoring of marine ecosystems and debris," *Journal of Applied Remote Sensing*, vol. 13, no. 4, pp. 1 – 10, 2019.

[6] J. Heidemann, M. Stojanovic, and M. Zorzi, "Underwater sensor networks: applications, advances and challenges," *Phil. Trans. R. Soc. A.*, vol. 370, pp. 158 – 175, 2012.

[7] T. Melodia, H. Kulhandjian, L. Kuo, and E. Demirors, "Advances in underwater acoustic networking," in *Mobile Ad Hoc Networking: Cutting Edge Directions*, 2nd ed., S. Basagni, M. Conti, S. Giordano, and I. Stojmenovic, Eds. Inc., Hoboken, NJ: John Wiley and Sons, 2013, pp. 804–852.

[8] F. Hanson and S. Radic, "High bandwidth underwater optical communication," *Applied Optics*, vol. 47, pp. 277–283, 2008.

[9] N. Cen, J. Jagannath, S. Moretti, Z. Guan, and T. Melodia, "Lanet: Visible-light ad hoc networks," *Ad Hoc Networks*, vol. 84, pp. 107 – 123, 2019.

[10] H. Kaushal and G. Kaddoum, "Underwater optical wireless communication," *IEEE Access*, vol. 4, pp. 1518–1547, 2016.

[11] J. W. Giles and I. N. Bankman, "Underwater optical communications systems. part 2: basic design considerations," in *IEEE MILCOM*, 2005, pp. 1700–1705 Vol. 3.

[12] N. Farr, A. Bowen, J. Ware, C. Pontbriand, and M. Tivey, "An integrated, underwater optical /acoustic communications system," in *IEEE OCEANS*, 2010, pp. 1–6.

[13] S. Q. Duntley, "Light in the sea*," *J. Opt. Soc. Am.*, vol. 53, no. 2, pp. 214–233, Feb 1963.

[14] M. Doniec, I. Vasilescu, M. Chitre, C. Detweiler, M. Hoffmann-Kuhnt, and D. Rus, "Aquaoptical: A lightweight device for high-rate long-range underwater point-to-point communication," in *OCEANS*, 2009, pp. 1–6.

[15] G. Cossu, R. Corsini, A. M. Khalid, S. Balestrino, A. Coppelli, A. Caiti, and E. Ciaramella, "Experimental demonstration of high speed underwater visible light communications," in *International Workshop on Optical Wireless Communications (IWOW)*, 2013, pp. 11–15.

[16] S. Hessien, S. C. Tokgöz, N. Anous, A. Boyacı, M. Abdallah, and K. A. Qaraqe, "Experimental evaluation of ofdm-based underwater visible light communication system," *IEEE Photonics Journal*, vol. 10, no. 5, pp. 1–13, 2018.

[17] M. Chen, P. Zou, L. Zhang, and N. Chi, "Demonstration of a 2.34 gbit/s real-time single silicon-substrate blue led-based underwater vlc system," *IEEE Photonics Journal*, vol. 12, no. 1, pp. 1–11, 2020.

[18] "Bluecomm underwater optical communication," 2021. [Online]. Available: https://tinyurl.com/1jpeixrn

[19] Z. Zeng, S. Fu, H. Zhang, Y. Dong, and J. Cheng, "A survey of underwater optical wireless communications," *IEEE Communications Surveys Tutorials*, vol. 19, no. 1, pp. 204–238, 2017.

[20] N. Chi and M. Shi, "Advanced modulation formats for underwater visible light communications," *Chin. Opt. Lett.*, vol. 16, no. 12, Dec 2018.

[21] X. Sun, M. Kong, O. A. Alkhazragi, K. Telegenov, M. Ouhssain, M. Sait, Y. Guo, B. H. Jones, J. S. Shamma, T. K. Ng, and B. S. Ooi, "Field demonstrations of wide-beam optical communications through water–air interface," *IEEE Access*, vol. 8, pp. 160 480–160 489, 2020.

[22] X. Sun, M. Kong, C. Shen, C. H. Kang, T. K. Ng, and B. S. Ooi, "On the realization of across wavy water-air-interface diffuse-line-of-sight communication based on an ultraviolet emitter," *Opt. Express*, vol. 27, no. 14, pp. 19 635–19 649, Jul 2019.

[23] M. S. Islam and M. F. Younis, "Analyzing visible light communication through air–water interface," *IEEE Access*, vol. 7, 2019.

[24] Y. Chen, M. Kong, T. Ali, J. Wang, R. Sarwar, J. Han, C. Guo, B. Sun, N. Deng, and J. Xu, "26 m/5.5 gbps air-water optical wireless communication based on an ofdm-modulated 520-nm laser diode," *Opt. Express*, vol. 25, no. 13, pp. 14 760–14 765, Jun 2017.

[25] P. Nabavi and M. Yuksel, "Performance analysis of air-to-water optical wireless communication using spads," in *IEEE Global Communications Conference (GLOBECOM)*, 2019, pp. 1–6.

[26] P. Nabavi, A. F. M. S. Haq, and M. Yuksel, "Empirical modeling and analysis of water-to-air optical wireless communication channels," in *IEEE International Conference on Communications Workshops (ICC Workshops)*, 2019, pp. 1–6.

[27] T. Lin, C. Gong, J. Luo, and Z. Xu, "Dynamic optical wireless communication channel characterization through air-water interface," in *IEEE/CIC ICCC Workshops*, 2020, pp. 173–178.

[28] F. Tonolini and F. Adib, "Networking across boundaries: Enabling wireless communication through the water-air interface," in *Proc. of ACM Special Interest Group on Data Communication (SIGCOMM)*, New York, NY, USA, 2018, p. 117–131.

[29] M. C. Domingo, "Magnetic induction for underwater wireless communication networks," *IEEE Transactions on Antennas and Propagation*, vol. 60, no. 6, pp. 2929–2939, 2012.

[30] I. F. Akyildiz, P. Wang, and Z. Sun, "Realizing underwater communication through magnetic induction," *IEEE Communications Magazine*, vol. 53, no. 11, pp. 42–48, 2015.

[31] M. Davies and A. K. Chattopadhyay, "Stokes waves revisited: Exact solutions in the asymptotic limit," *The European Physical Journal Plus*, vol. 131, no. 3, p. 69, Mar 2016.

[32] W. Cox and J. Muth, "Simulating channel losses in an underwater optical communication system," *J. Opt. Soc. Am. A*, vol. 31, no. 5, pp. 920–934, May 2014.

[33] K. O. Akande, P. A. Haigh, and W. O. Popoola, "On the implementation of carrierless amplitude and phase modulation in visible light communication," *IEEE Access*, vol. 6, pp. 60 532–60 546, 2018.

[34] Z. Wang, T. Mao, and Q. Wang, "Optical ofdm for visible light communications," in *2017 13th International Wireless Communications and Mobile Computing Conference (IWCMC)*, 2017, pp. 1190–1194.

[35] O. of Water Regulations and Standards, *Turbidity / Water Quality Standards Criteria Summaries: A Compilation of State/Federal Criteria*. EPA, 1988.